Frost Formation: Optimizing solutions under a finite volume approach

E Bartrons, C D Perez-Segarra and C Oliet

Heat and Mass Transfer Technological Center (CTTC), Universitat Politècnica de Catalunya (UPC), ESEIAAT, Carrer de Colom 11, 08222 Terrassa (Barcelona), Spain.

E-mail: cttc@cttc.upc.edu

Abstract.

A three-dimensional transient formulation of the frost formation process is developed by means of a finite volume approach. Emphasis is put on the frost surface boundary condition as well as the wide range of empirical correlations related to the thermophysical and transport properties of frost. A study of the numerical solution is made, establishing the parameters that ensure grid independence. Attention is given to the algorithm, the discretised equations and the code optimization through dynamic relaxation techniques. A critical analysis of four cases is carried out by comparing solutions of several empirical models against tested experiments. As a result, a discussion on the performance of such parameters is started and a proposal of the most suitable models is presented.

1. Introduction

Whenever a surface is in contact with humid air below the dew and freezing points, water vapor will transition to a solid state forming a crystaline structure called frost. This common phenomenon has a great impact on the aerospace, cryogenics and refrigeration industry among others.

Hayashi et al. [1] divided the frost formation mechanism into three periods: the *crystal growth period*, the *frost layer growth period* and the *frost layer full growth period*. The first refers to an early growth period characterized by crystal growth. In the second period, the rough frost grows into a more uniform layer: crystals continue growing while interacting with each other. This period ends when the thickness of the frost stops growing. The third period continues with an increase of thermal resistance (which leads to a stop of thickness growth at the expenses of densificating the frost layer), until the frost surface reaches the melting point. The frost surface begins to melt, and the melted water soaks into the frost layer, which freezes in the inside. The melting and freezing lowers the frost thermal resistance, allowing new frost deposition and thus an increase of the frost layer thickness. This cycle process continues periodically until the heat transfer condition reaches the equilibrium.

The frost layer growth period is the most studied among the three. Brian et al. [2] proposed first analytical approximations to model frost growth. Later on, Tao et al. [3] and Le Gall et al. [4] introduced an averaged finite volume approach.

Despite the large number of frost growth modeling articles in the literature, just few authors (see Kandula [5]) have compared their model with experimental data from other works on a wide range of experiments. In view of the reported results, a new finite volume approach that

models the frost layer growth period (until the melting point is reached) on a 3D perspective is presented, aiming to provide a robust and reliable solution in a considerable range of conditions.

2. Mathematical formulation

The approach is set out through a local averaged control volume analysis. This technique considers that a volume V is equal to the summation of the ice V_i and humid air V_{ha} contained in it. The porosity is then either defined as an ice porosity $\varepsilon_i = V_i/V$ or an air porosity $\varepsilon_{ha} = V_{\mathrm{ha}}/V$ such that $\varepsilon_{\mathrm{ha}} + \varepsilon_i = 1$. From this point onwards, the humid air porosity ε_{ha}, the water vapor porosity ε_v or just ε will be used interchangeably.

The assumptions made in the present analysis are: (a) the total gas phase pressure P_{ha} is constant throughout the porous frost layer and equal to the external atmospheric pressure P_∞; (b) water vapor, dry air and ice are in local thermal equilibrium, i.e., $T_{\mathrm{ha}} = T_v = T_{\mathrm{da}} = T_i$; (c) water vapor inside the frost layer is saturated; (d) the heat and mass transfer analogy is applicable, with a constant Lewis number; (e) convection effects are negligible such that $\vec{v}_{\mathrm{ha}} \approx 0$ within the frost layer [6]; (f) no movement of the ice crystals is allowed ($\vec{v}_i = 0$).

2.1. The vapor diffusion equation

The vapor mass conservation equation is given by the following equation:

$$\frac{\partial}{\partial t}\int_{V_v} \rho_v \mathrm{d}V_v + \oint_{S_v} \rho_v \left(\vec{v}_v - \vec{v}_b\right)\cdot\vec{n}\mathrm{d}S_v = \int_V \dot{\omega}_v \mathrm{d}V \tag{1}$$

where the Left Hand Side (LHS) of the equation refers to the substantial derivative of the Eulerian density field including the volume swept by the mesh, and the Right Hand Side (RHS) refers to the generation or destruction of water vapor. Integrating over the volume V and introducing the Fick's law:

$$\frac{\partial}{\partial t}\int_V \rho_v\varepsilon_v \mathrm{d}V + \oint_S \rho_v\varepsilon_v \left(\vec{v} - \vec{v}_b\right)\cdot\vec{n}\mathrm{d}S = \int_S \rho_{ha}\varepsilon_v\tau D_v \nabla Y_v\cdot\vec{n}\mathrm{d}S + \int_V \dot{\omega}_v \mathrm{d}V \tag{2}$$

where Y_v is the concentration of water vapor and $\tau\left(\varepsilon\right)$ is the tortuosity. The effective diffusivity is defined as $D_{\mathrm{eff}} \equiv \varepsilon_v\tau D_v$, where the diffusion resistance factor $\mu\left(\varepsilon\right)$ is equal to $\varepsilon_v\tau$. On the other hand, the mass conservation equation of the ice phase reads as:

$$\frac{\partial}{\partial t}\int_V \rho_i\varepsilon_i \mathrm{d}V + \oint_S \rho_i\varepsilon_i \left(\vec{v}_i - \vec{v}_b\right)\cdot\vec{n}\mathrm{d}S = \int_V \dot{\omega}_i \mathrm{d}V \tag{3}$$

where ice generation equals water vapor destruction. The equation 2 is then rearranged as follows:

$$\frac{\partial}{\partial t}\int_V \varepsilon_v\left(\rho_v - \rho_i\right)\mathrm{d}V - \oint_S \varepsilon_v\left(\rho_v - \rho_i\right)\vec{v}_b\cdot\vec{n}\mathrm{d}S = \oint_S \rho_i\vec{v}_b\vec{n}\mathrm{d}S - \frac{\partial}{\partial t}\int_V \rho_i\mathrm{d}V + \oint_S \rho_{ha}D_{\mathrm{eff}}\nabla Y_v\vec{n}\mathrm{d}S \tag{4}$$

2.2. The energy equation

The energy conservation equation is given by the following equation:

$$\underbrace{\frac{\partial}{\partial t}\int_V \sum \rho_k\left(h_k - \frac{P_k}{\rho_k}\right)\mathrm{d}V_k}_{(I)} + \underbrace{\oint_S \sum \rho_k h_k\left(\vec{v}_k - \vec{v}_b\right)\cdot\vec{n}\mathrm{d}S_k}_{(II)} = \underbrace{-\oint_S \sum \vec{q}_k\cdot\vec{n}\mathrm{d}S_k}_{(III)} \tag{5}$$

where $k = \{i, \mathrm{ha}\}$. Humid air enthalpy is a mixture of water vapor and dry air enthalpies, i.e., $h_{\mathrm{ha}} = Y_v h_v + (1 - Y_v)\, h_{\mathrm{da}}$. Enthalpies are defined as:

$$h_n = h_{f_n} + \int_{T_{\mathrm{ref}}}^{T} c_{p_i} \mathrm{d}T \approx h_{f_n} + \bar{c}_{p_n} \left(T - T_{\mathrm{ref}}\right) \quad ; \quad \bar{c}_{p_n} = \frac{1}{T - T_{\mathrm{ref}}} \int_{T_{\mathrm{ref}}}^{T} c_{p_n} \mathrm{d}T \tag{6}$$

where $n = \{i, v, \mathrm{da}\}$ and h_f is the formation enthalpy. Rearranging the terms of equation 5, the following expression is reached:

$$\begin{aligned} \frac{\partial}{\partial t} \int_V \left(\mathcal{C}_1 T + \mathcal{C}_2 \varepsilon + \mathcal{C}_3 \varepsilon T\right) \mathrm{d}V - \oint_S \left(\mathcal{C}_1 T + \mathcal{C}_2 \varepsilon + \mathcal{C}_3 \varepsilon T\right) \vec{v}_b \cdot \vec{n} \mathrm{d}S = \\ \oint_S \left(\mathcal{C}_4 + P_\infty\right) \vec{v}_b \cdot \vec{n} \mathrm{d}S + \oint_S \lambda_{\mathrm{fl}} \nabla T \vec{n} \mathrm{d}S - \frac{\partial}{\partial t} \int_V \mathcal{C}_4 \mathrm{d}V \end{aligned} \tag{7}$$

where λ_{fl} is the frost layer (fl) conductivity and the constants $\mathcal{C}_1, \mathcal{C}_2, \mathcal{C}_3, \mathcal{C}_4$ are given by:

$$\begin{aligned} \mathcal{C}_1 &= \rho_i \bar{c}_{p_i} + \rho_{\mathrm{ha}} \bar{c}_{p_v} \\ \mathcal{C}_2 &= \rho_i \left(\bar{c}_{p_i} T_{\mathrm{ref}_i} - h_{f_i}\right) + \rho_{\mathrm{ha}} \bar{c}_{p_{\mathrm{da}}} T_{\mathrm{ref}_{\mathrm{da}}} \left(Y_v - 1\right) \\ \mathcal{C}_3 &= \rho_{\mathrm{ha}} \bar{c}_{p_{\mathrm{da}}} \left(1 - Y_v\right) - \rho_i \bar{c}_{p_i} \\ \mathcal{C}_4 &= \rho_i \left(h_{f_i} - \bar{c}_{p_i} T_{\mathrm{ref}_i}\right) + \rho_{\mathrm{ha}} Y_v \left(h_{f_v} - \bar{c}_{p_v} T_{\mathrm{ref}_v}\right) - P_\infty \end{aligned}$$

2.3. Boundary conditions

Air-frost interface: The temperature at the frost surface (fs) is calculated by means of an energy balance at the interface:

$$\lambda_{\mathrm{fl}} \frac{\partial T_{\mathrm{fl}}}{\partial n} = h_c \left(T_\infty - T_{\mathrm{fs}}\right) + \rho_{\mathrm{fl}} \Delta h_{\mathrm{sv}} \frac{\mathrm{d}y_{\mathrm{fs}}}{\mathrm{d}t} \tag{8}$$

where the LHS term is the sensible heat that penetrates into the frost layer, the first RHS term is the total heat flux reaching the frost surface from the air side, and the second RHS term refers to the latent heat due to phase transition. Nusselt numbers used for the present study are the ones proposed by Wong [7].

A mass balance over the frost interface gives:

$$\rho_{\mathrm{fl}} \frac{\mathrm{d}y_{\mathrm{fs}}}{\mathrm{d}t} = h_m \left(\rho_{v_\infty} - \rho_{v_{\mathrm{fs}}}\right) - \rho_{\mathrm{ha}} D_{\mathrm{eff}} \frac{\partial Y_{v,\mathrm{fl}}}{\partial n} \tag{9}$$

Notice that the total deposited mass (first RHS term) splits into the part that contributes to the thickness growth (LHS term) and the one that densifies the frost layer (second RHS term).

One of the main issues is associated to the calculation of the water vapor pressure at the frost surface. Although theoretical analyses state the water vapor must be supersaturated for the phase change to occur, no method for the calculation of such pressure values has yet been reported. Authors (e.g. [4, 8]) prior to Na and Web used a saturation condition, while the latter suggested an empirical expression extracted from linearizing the laminar boundary layer equations (see [9]). Later on, Kandula [5] used again a saturation condition claiming that the supersaturation degree is strongly dependent to the surface coating governing the contact angle and that there is no such information in the reported experimental data.

Another condition was recently used by El Cheikh and Jacobi [10], which uses the total air heat flux acquired at the frost surface. Unfortunately, this condition needs such value from the experiment.

For the purposes of the present study, that focuses on giving a fully independent model of frost formation, El Cheikh and Jacobi's condition was not considered and saturated and supersaturated conditions were tested.

Referring to the frost density, the Neumann-type condition used by Na and Webb [11] is applied, i.e, $\partial\rho_{\mathrm{fl}}/\partial n|_{\mathrm{fs}} = 0$.

The solid wall: The wall is kept at a constant temperature $T = T_w$ and it is totally impermeable, such that the water vapor concentration gradient is zero, thus, $\partial Y_v/\partial n|_{\mathrm{w}} = 0$. Moreover, there is no change in porosity, which leads to $\partial\varepsilon_v/\partial n|_{\mathrm{w}} = 0$.

Other boundaries: Neumann-type boundary conditions are chosen for the temperature, water vapor concentration and porosity.

3. Numerical Solution

The pair $\{T, \varepsilon\}$ is solved using a common finite volume method. Temporal derivatives are discretized with forward Euler temporal schemes. Discretization of face values at previous time instant t^n is performed with Central Difference Schemes (CDS) whereas face values at current time t^{n+1} are delt with higher diffusive schemes such as first order Upwind Differential Schemes (UDS) due to instabilities that may arise near the wall. The frost layer conductivity at the faces has been calculated by means of the well known harmonic mean.

The algorithm, which follows a fully implicit time resolution, is presented below:

(1) Initial contitions: $\{\bar{T}_{\mathrm{fl}} = T_w\ ;\ y_{\mathrm{fs}}^0 = 10^{-5}\ \mathrm{m}\ ;\ \bar{\rho}_{\mathrm{fl}}^0$ (see table 1)$\}$
(2) New time step Δt. If $t_{\mathrm{sim}} > t_{\mathrm{end}} \Rightarrow$ End of Simulation.
(3) Calculate $\Delta y_{\mathrm{fs}}^{n+1}$.
(4) Check $\frac{\|^{\ell}\Delta y_{\mathrm{fs}}^{n+1} - ^{\ell-1}\Delta y_{\mathrm{fs}}^{n+1}\|}{\|^{\ell}\Delta y_{\mathrm{fs}}^{n+1}\|} < \delta_1$. If YES, go to number 2.
(5) Move mesh.
(6) Calculate T.
(7) Update physical properties.
(8) Calculate ε.
(9) Update physical properties.
(10) Check $\frac{\|^{m}T^{n+1} - ^{m-1}T^{n+1}\|}{\|^{m-1}T^{n+1}\|} < \delta_2$ && $\frac{\|^{m}\varepsilon^{n+1} - ^{m-1}\varepsilon^{n+1}\|}{\|^{m-1}\varepsilon^{n+1}\|} < \delta_2$.
If NO, ${}^{m}T^{n+1,\mathrm{NEW}} = f\left({}^{m-1}T^{n+1}, {}^{m}T^{n+1}, fr\right)$ and ${}^{m}\varepsilon^{n+1,\mathrm{NEW}} = f\left({}^{m-1}\varepsilon^{n+1}, {}^{m}\varepsilon^{n+1}, fr\right)$ and go to number 6.
(11) ${}^{m}T^{n+1,\mathrm{NEW}} = {}^{m}T^{n+1}$ and ${}^{m}\varepsilon^{n+1,\mathrm{NEW}} = {}^{m}\varepsilon^{n+1}$ and go to number 3.

Where ℓ refers to the current outer iteration and m refers to the inner iteration. fr refers to the underelaxation factors, implemented as dynamic relaxation factors using the Aitken's Δ^2 method.

The movement of the mesh encloses steps 3, 4 and 5 of the algorithm. There is no refinement of the mesh, making each control volume to readapt at each subiteration. Figure 1 shows an example of a moving pattern followed within a time step. In this example, note that the algorithm goes through number 5 twice before the $\Delta y_{\mathrm{fs}}^{n+1}$ convergence is reached.

Table 1. List of parameters tested in each case.

Parameter	Value-Correlation
D_{eff}	{ Auracher [13], Prager [14], Zehnder [15], Brugeman [14], Le Gall [4] with $F = \{1, 1.5, 2, 2.5, 3, 3.5\}$ }
λ_{fl}	{ Na and Webb [9], Lee [16], Negrelli [17] }
ρ^0_{fl}	$\{25, 30, 35\}$ kg/m^3
Le	{0.905[8],1}
P_{fs}	{Saturated, Supersaturated}

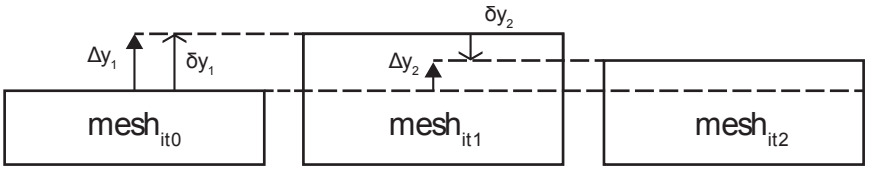

Figure 1. Schematized pattern of a 2-iteration mesh movement.

Δy is the total amount of frost thickness that the frost layer accumulates at a certain time step. While Δy has a physical meaning, δy is purely geometrical and represents the amount that the mesh has to move at a specific outer iteration.

$$\delta y_{\text{subit}} =^{\ell} \Delta y_{\text{fs}}^{n+1} -^{\ell-1} \Delta y_{\text{fs}}^{n+1} \tag{10}$$

Notice that Δy is positive-definite, while δy can take either positive or negative values. The technique used to perform the movement of the mesh is based on a classical elasticity-based mesh update model proposed by Smith and Wright [12].

The $\delta' s$ that appear in steps 4 and 10 refer to the convergence criteria. The later are studied along with the time step and the mesh size in order to secure grid independence. The adequate values found are a time step of $10^{-2}s$ and the pair $\{\delta_1 = 10^{-5}\ ;\ \delta_2 = 10^{-4}\}$ under a 30-cell mesh.

4. Numerical Results

The presented model needs several empirical inputs. These are the effective diffusivity, the frost layer conductivity, the initial frost mean density, the Lewis number and the pressure condition at the air-frost interface. Several empirical correlations have been proposed in the literature, however, these show differences among each other. Such differences urge to conduct parametric studies by means of the introduced model in order to determine a combination that gives best fits against tested experimental data. The empirical correlations and simulation parameters used are given in table 1.

There is an extensive literature with experimental results uniquely related to frost thickness. Few articles report frost mean density measurements and rarely frost surface temperature data is provided. Taking into account the preference of selecting cases with data of these three variables (recall its strong coupling seen in section 2) while covering the typical range of experimental conditions in which frost formation has been experimentally tested, four cases were chosen (see table 2).

Due to the large number of results, an statistical post-process which consists on calculating the R-squared value of each graph (thickness, mean density, surface temperature) is made after every simulation in order to find out the best fits of each case.

Table 2. Chosen experimental conditions and measured data based on Lee et al. [8] and Lee and Ro [18] experiments.

Case	W (kg_v/kg_{da})	T_w (°C)	T_∞ (°C)	v (m/s)	Data
C1 [8]	0.00531	−20	10	1.75	$\{y_{\text{fs}}; \bar{\rho}_{\text{fl}}; T_{\text{fs}}\}$
C2 [8]	0.00637	−15	15	2.5	$\{y_{\text{fs}}; \bar{\rho}_{\text{fl}}; T_{\text{fs}}\}$
C3 [8]	0.00323	−15	5	1	$\{y_{\text{fs}}; \bar{\rho}_{\text{fl}}; T_{\text{fs}}\}$
C4 [18]	0.003	−20	5	1.46	$\{y_{\text{fs}}; \bar{\rho}_{\text{fl}}\}$

Table 3. Best fit cases.

Case	D_{eff}	λ_{eff}	ρ^0_{fl} $\left(kg/m^3\right)$	Le	P_{fs}
C1-C2-C3-C4	Le Gall [4] with $F = 3$	Na and Webb [9]	35	1	Sat.
C1	Le Gall [4] with $F = 3$	Na and Webb [9]	35	1	Sat.
C2	Le Gall [4] with $F = 3$	Na and Webb [9]	35	1	Sat.
C3	Le Gall [4] with $F = 3.5$	Na and Webb [9]	25	0.905	Super-Sat.
C4	Le Gall [4] with $F = 3.5$	Na and Webb [9]	35	0.905	Sat.

4.1. Numerical Assessment of the Empirical Inputs

As will be seen, there exist plenty of combinations that give good fittings of the frost layer thickness evolution, although few of them capture the rest of the properties with acceptable discrepancies. Testing a model uniquely against frost thickness measurements does not ensure, by any means, a proper capture of the physical phenomenon.

Both the thickness and the frost mean density are global values of the problem, which are linked together. Whenever using parameters that give an increase to the thickness, the mean frost density decreases and viceversa. On the other hand, the surface temperature is much more sensitive to parameter changes (notice the large variations among its solutions in figure 2). As a consequence, it was decided to give more weight to the first two variables (y_{fs} and $\bar{\rho}_{\text{fl}}$), while maintaining, whenever possible, an acceptable R-squared value of the surface temperature graph. The best combination was then found by maximizing the sum of the R-squared values of the thickness and the mean density of the four cases (see table 3).

A compilation of the cases simulated with Le Gall's [4] effective diffusivity ($\mu > 1$) is shown in figure 2 as a guide to understanding the influence of the tested parameters on the final R-squared values. In general, the results show that the combinations match quite frequently the behaviour of the frost growth, whereas proper matches of the frost mean density and the frost surface temperature are more scarce. In cases C1, C2 and C3 shown in figure 2, there are 278 runs that have thickness R-squared values above zero, 151 for the frost mean density and 75 for the surface temperature. Moreover, 150 runs have both positive thickness and mean density R-squared values, while just 41 of them have the three positive R-squared values.

The periodicities seen in figure 2 show that the best results are given when the frost layer conductivity correlation is the one stated by Na and Webb [11] whereas the rest of the correlations do not manifest notable differences among each other. It also shows that results get better when enlarging either the factor F of Le Gall's [4] correlation and the frost mean density. Moreover, using the saturated condition allows overall better approximations while no important changes

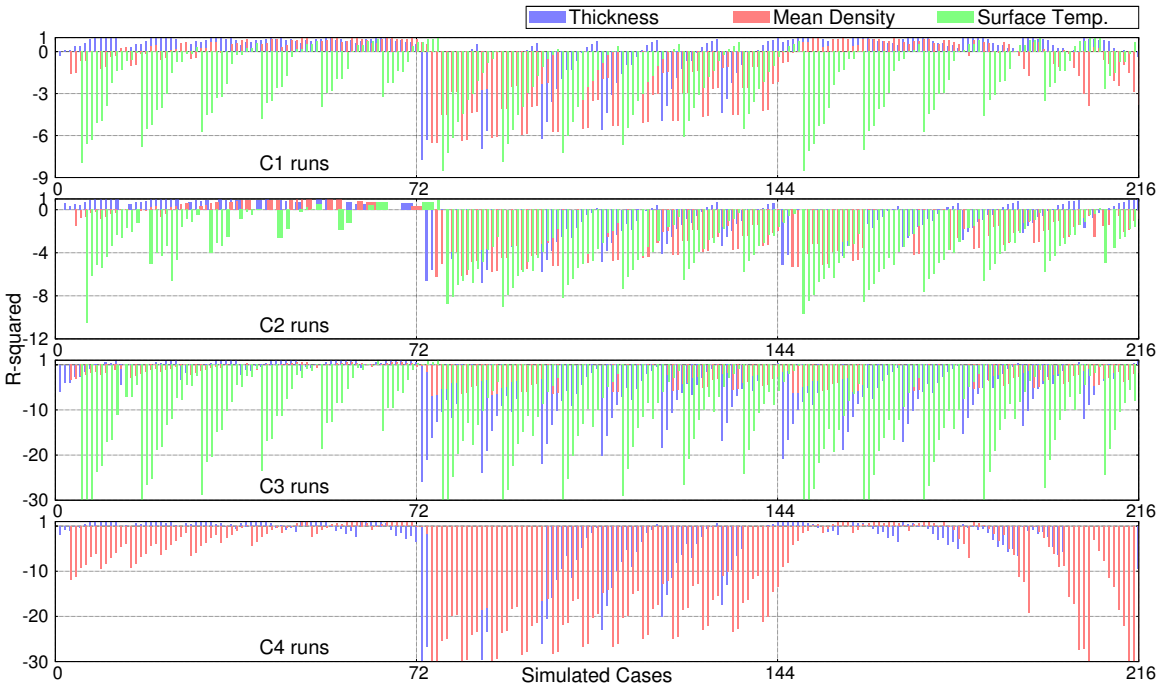

Figure 2. R-squared values of C1, C2, C3 and C4 runs with Le Gall's [4] effective diffusivity. Changes of λ_{eff}, $\bar{\rho}_{\text{fl}}$, F factor, Le and P_{fs} condition are given every 72, 2, 12, 1 and 6 runs respectively. Periodicities of $\bar{\rho}_{\text{fl}}$, F factor and P_{fs} are given every 6, 72 and 12 runs respectively.

are appreciated when changing the Lewis number from 1 to 0.905. This patterns are also encountered in the rest of the parametric cases.

On the other hand, Auracher, Prager, Zehnder and Brugeman effective diffusivities ($\mu < 1$) show worse results than Le Gall's correlation. Some of them provide good agreement of the frost growth although lack a proper capture of the other two variables that usually follow the tendency line although shifted. This is due to the lower ratio observed between the calculated deposited mass and the experiment deposited mass compared to the one resulting from a $\mu > 1$ effective diffusivity. Indeed, it difficult not to underestimate the mean frost density when having a good fit of the frost thickness and viceversa.

5. Conclusions

Tackling the problem of frost formation is still a challenge. Despite the many empirical correlations proposed in literature, there is not yet agreement on which combinations of parameters capture better the formation pattern. A detailed assessment of these parameters has been carried out, resulting on a combination that ensure best fits under the tested experimental conditions. This combination uses Le Gall's effective diffusivity, Na and Webb's frost layer conductivity and a saturated condition at the air-frost interface. Moreover, not only the volatility of the model when using certain sets of parameters is manifested, but also a set of recommendations is given.

Acknowledgments

This work has been financially supported by the Ministerio de Economía y Competitividad, Secretaría de Estado de Investigación, Desarrollo e Innovación, Spain (Project VAPFLOW, ENE-2012-36910).

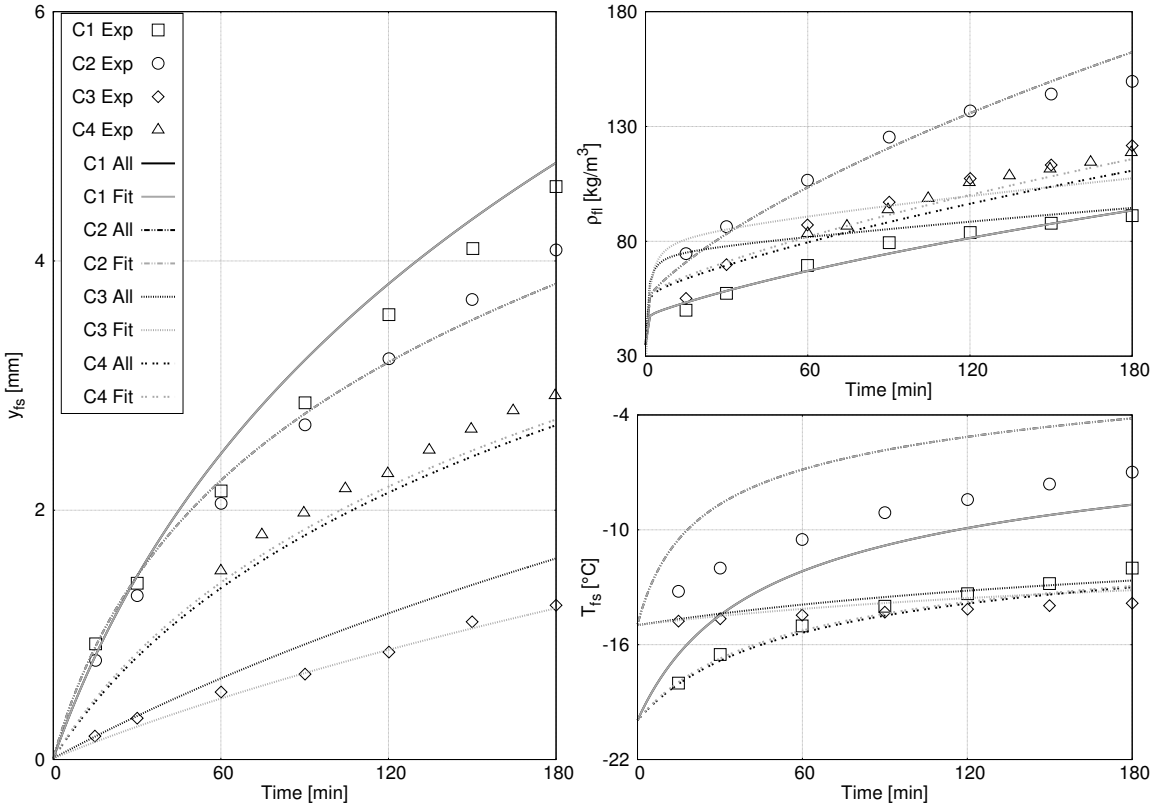

Figure 3. Thickness, frost mean density and temperature evolution of the frost layer for the tested cases. *All* refers to C1-C2-C3-C4 best fit and *Fit* refers to the case's best fit (see table 3).

References

[1] Hayashi Y, Aoki A, Adaohi S and Hori K 1977 *J. Heat Transfer* **99** 239–45
[2] Brian P L T, Reid R C and Shah Y T 1970 *Ind. Eng. Chem. Fundam.* **9** 375–80
[3] Tao Y X, Besant R and Rezkallah K 1993 *Int. J. Heat Mass Transf.* **36** 353–63
[4] Gall R L, Grillot J and Jallut C 1997 *Int. J. Heat Mass Transf.* **40** 3177–87
[5] Kandula M 2011 *Int. J. Heat Mass Transf.* **54** 3719–31
[6] Woodside W 1958 *Can. J. Phys.* **36** 815–23
[7] Wong H 1977 *Handbook of Essential Formulae and Data on Heat Transfer for Engineers* (London: Longman)
[8] Lee K S, Jhee S and Yang D K 2003 *Int. J. Heat Mass Transf.* **46** 3789–96
[9] Na B and Webb R L 2004 *Int. J. Heat Mass Transf.* **47** 899–911
[10] Cheikh A E and Jacobi A 2014 *Int. J. Heat Mass Transf.* **77** 604–11
[11] Na B and Webb R L 2004 *Int. J. Heat Mass Transf.* **47** 925–36
[12] Smith R W and Wright J A 2010 *48th AIAA Aerospace Sciences Meeting Including the New Horizons Forum and Aerospace Exposition, Orlando, Florida, Jan. 4-7* pp 2010–164
[13] Auracher H 1972 *Bulletin of the International Institute of Refrigeration* pp 477–88
[14] Cunningham R and Williams R 1980 *Diffusion in Gases and Porous Media* (New York: Plenum Press)
[15] Sanders C T 1974 Ph.D. thesis Technische Hogeschool, Delft (Netherlands)
[16] K S Lee T H Lee W S K 1994 *Korean J. Air Cond. Refrig. Eng.* **6** 155–65
[17] Negrelli S and Hermes C J 2015 *Int. J. Refrig.* **58** 243–52
[18] Lee Y and Ro S 2005 *Exp. Therm. Fluid Sci.* **29** 685–96